J. Fluid Mech. (1990), *vol.* 219, *pp.* 387–404
Printed in Great Britain

The vortices of geostrophic turbulence

By JAMES C. McWILLIAMS
Geophysical Turbulence Program, National Center for Atmospheric Research,
PO Box 3000, Boulder, CO 80307, USA

(Received 16 May 1989 and in revised form 20 March 1990)

A solution for decaying geostrophic turbulence at large Reynolds number is analysed by means of an automated vortex census. The census identifies the flow structures that approximately conform to the idealized shape of an isolated, coherent geostrophic vortex. It also determines vortex characteristics, such as amplitude, size, and shape. The distributions of these characteristics within the vortex population are examined, as are their time evolutions. These distributions are interpreted with reference to the dynamical processes of vortices, and they are compared to analogous distributions from a solution for two-dimensional turbulence.

1. Introduction

Geostrophic turbulence – the turbulence of three-dimensional, rotating, stably stratified flow – is believed to be a useful idealization of many planetary-scale flows, and it is often thought of as a more complex form of two-dimensional turbulence (Charney 1971; Rhines 1979). Among the many shared properties of these two types of flow is the spontaneous development of long-lived, isolated concentrations of vorticity, also called coherent vortices.

This paper is concerned with the identification and measurement of the coherent vortices in a numerical solution for the free decay of geostrophic turbulence at high Reynolds number (i.e. such that the energy decay is small over many advective time units), and is an extension of two other, recent studies by the author. Since the overlap is considerable, the present paper is written with the assumption that readers have access to the others, in order to avoid unnecessary repetition.

The first one (McWilliams 1989, hereinafter referred to as DGT) is an investigation of the statistical properties of decaying geostrophic turbulence. These properties include inverse energy transfer (i.e. transfer to larger horizontal and vertical scales), modest energy dissipation together with substantial enstrophy dissipation, approximate three-dimensional isotropy of energy and enstrophy spectra, persistence of vertical inhomogeneity, and the emergence of coherent vortices which subsequently dominate the flow evolution. The present vortex analysis is made on the principal solution in DGT, which is there referred to as solution A, and table 1 contains some of its statistical measures that illustrate the behaviour described above. This particular solution is typical of the broad class of solutions examined in DGT. Also, the reader is referred to DGT for presentations of the geostrophic model and the techniques for its numerical solution.

The second companion study (McWilliams 1990*a*, hereinafter referred to as V2D) identifies and measures the properties of coherent vortices in a numerical solution of decaying two-dimensional turbulence. Its methodology is quite close to that used here, and, as anticipated above, the vortex properties it demonstrates are essentially

t	T	V	μ_v	Ku_q
	1.000	1716.0	52.2	3.0
0.1	0.976	1595.0	53.0	3.1
0.3	0.910	1226.0	52.9	3.2
1.0	0.782	515.0	45.4	3.7
3.0	0.708	131.0	31.6	6.4
10.0	0.683	28.7	19.1	27.0
30.0	0.675	10.7	12.0	69.0

The quantities in this table are defined below. For further definitions refer to DGT.

$$T = \frac{1}{4\pi^3}\int\int\int \mathrm{d}\boldsymbol{x}\tfrac{1}{2}\left(\psi_x^2+\psi_y^2+\frac{f^2}{N^2}\psi_z^2\right),$$

$$V = \frac{1}{4\pi^3}\int\int\int \mathrm{d}\boldsymbol{x}\tfrac{1}{2}q^2 = \int\int\int \mathrm{d}\boldsymbol{k}\hat{V}(\boldsymbol{k}),$$

$$q = \psi_{xx}+\psi_{yy}+\frac{f^2}{N^2}\psi_{zz},$$

$$\mu_v = \frac{\int\int\int \mathrm{d}\boldsymbol{k}(k_x^2+k_y^2+N^2/f^2\,k_z^2)^{\frac{1}{2}}\hat{V}(\boldsymbol{k})}{\int\int\int \mathrm{d}\boldsymbol{k}\,\hat{V}(\boldsymbol{k})},$$

$$ku_q = \frac{\int\int\int \mathrm{d}\boldsymbol{x}\,q^4}{[\int\int\int \mathrm{d}\boldsymbol{x}\,q^2]^2}$$

TABLE 1. Solution properties

similar to many of those found here. Of course, it is the horizontal coordinates (x, y) for which there is the greatest similarity with two-dimensional turbulence in methodology and vortex structure and behaviour, whereas attributes related to the vertical coordinate z are unique to geostrophic turbulence.

The measurement of vortex properties in turbulence is complementary to analyses of their dynamical processes: the former exposes the consequences of the latter. Many of the dynamical processes of geostrophic vortices are well known, among which are those shared with two-dimensional vortices, albeit with modifications due to non-trivial vertical structure: barotropic stability limits on vortex shape in horizontal planes; viscous decay of amplitude and diffusive spreading of the spatial flow patterns; vortex emergence and horizontal organization of the flow patterns through axisymmetrization of vorticity patches (i.e. regions with a dominant sign in the vorticity field) about their extrema; horizontal deformation and filamentation and enhanced viscous dissipation in response to horizontal strain (i.e. $S_h = [(u_x-v_y)^2+(u_y+v_x)^2]^{\frac{1}{2}}$, where (u, v) are the horizontal velocity components); mutual advection (as among point vortices); apparently stable aggregations of opposite-sign vorticity patches (e.g. dipoles and tripoles); and merger of like-sign vortices. These processes have a lengthy history of investigation, especially in a two-dimensional context (see V2D); a survey of their investigation in a geostrophic context is made in McWilliams (1990*b*).

In addition, there are other dynamical processes peculiar to geostrophic vortices. These include baroclinic (e.g. Flierl 1988) and internal barotropic (e.g. Gent & McWilliams 1986) instability limits on vortex shape; structural organization through

vertical alignment of the axis connecting the horizontal extrema of vorticity (Polvani 1990); deformation away from vertical alignment, vertical fragmentation, and enhanced viscous dissipation in response to vertical strain (i.e. $S_v = (u_z^2 + v_z^2)^{\frac{1}{2}}$ – in geostrophic flow the vorticity and strain associated with the vertical velocity w are negligible); conversion among the components of potential vorticity to cause the migration of vorticity extrema towards vertical boundaries; and attachment of like-sign vortices whose three-dimensional extrema are at different vertical levels. For the most part, these processes have simply been observed to occur (see DGT), and there is still much to be learned about geostrophic vortex dynamics. For the purposes of this paper, it must suffice to make qualitative associations between the measured vortex properties and their evolution and our heuristic understanding of geostrophic vortex dynamics.

2. Vortex selection procedure

We seek an analysis procedure for numerical solutions of geostrophic turbulence that identifies the coherent vortices present and then measure their properties. The identification or selection criteria are based upon an assumed archetypal vortex structure: the vertical component of vorticity is of one sign in a three-dimensional region about a central extremum; the axis connecting horizontal extrema at different vertical levels is aligned vertically; and the vorticity distribution is axisymmetric about a single extremum in each of the horizontal planes perpendicular to the axis. The aptness of this structure is illustrated in figures 9 and 10 of DGT. In particular, we choose the vorticity ζ, rather than the advectively conserved potential vorticity q, as the field from which to select the coherent vortices. The reasons for this, as described in DGT, are that the distribution of ζ in coherent vortices is primarily of only one sign whereas q has connected zones of alternating sign, and ζ is more compactly distributed in space than is q.

The selection procedure is a generalization of the one in V2D. The general rationale for the procedure is presented in §3 of V2D and will not be repeated here. All aspects referring to the horizontal plane containing the central extremum are identical with those in V2D. All additions to the procedure refer to the axis. For simplicity, we do not analyse the vorticity in horizontal planes other than the one with the central extremum. This axis-and-plane scheme is illustrated in figure 1.

The analysis is made on the spatially gridded vertical vorticity field $\zeta(x, y, z)$ at a sequence of times from Solution A of DGT. The horizontal and vertical grid intervals are $\mathrm{d}s = 2\pi/N_x = 0.0327$ and $\mathrm{d}z = \pi/N_z = 0.0982$. The spatial domain is horizontally periodic and vertically bounded, with $0 \leqslant x, y \leqslant 2\pi$, $0 \leqslant z \leqslant \pi$. The time sequence consists of all unit times $0 \leqslant t \leqslant 30$ plus $t = 0.5$ to better resolve the early stages of vortex emergence.

The selection procedure is the following:

A. *Identify extrema* Vortices are required to have a three-dimensional extremum in vorticity as their centre, with an amplitude above a specified threshold value.

Procedure Determine the amplitudes ζ_n and positions (x_n, y_n, z_n), $n = 1, \ldots, N_e$, for all extrema above a threshold value $\zeta_{\min}$. The extrema are placed in order of decreasing amplitude. The extremum test further requires that a candidate extremum have the largest magnitude within a local volume with dimensions $L_e \times L_e \times 3\mathrm{d}z$, unless z_n is on a vertical boundary, in which case the height of the test volume is $2\mathrm{d}z$ directed only into the interior.

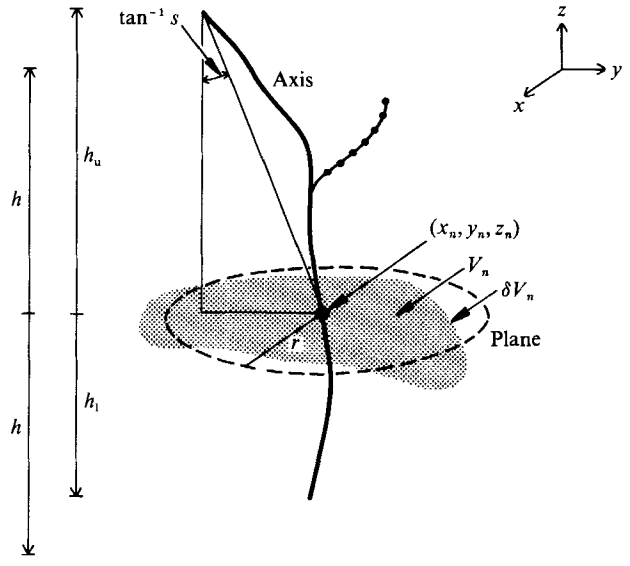

FIGURE 1. Axis-and-plane analysis scheme. The large black dot denotes the central vorticity extremum, the stippled region denotes the vortex interior in the plane of the central extremum, the solid line denotes the axis, and the line with dots denotes a secondary axis branch discarded during the elimination of redundancy. See text for further definitions.

Comments We choose $L_e = 4ds$ and $\zeta_{min} = 10$, as in V2D.

B. *Identify axes* A vortex axis is a connected line of like-sign horizontal extrema in ζ, not excessively tilted away from a vertical alignment.

Procedure For each n in sequence, a search is made in z outward from the core, first up then down. At each step in the search a point is accepted as on the axis if it is a local horizontal extremum, if it lies within a square of length L_e centred at the horizontal position of the last-accepted axis point next closest to the centre, and if it satisfies

$$\frac{\zeta}{\zeta_n} \geqslant \Delta. \tag{1}$$

If any of these tests is failed, the axis is terminated at the last accepted point. It also is terminated once a vertical boundary point is accepted.

Comments The issue of vertical connectedness is somewhat problematic. The second criterion above implies that local axis slopes (ratio of horizontal and vertical displacements of vertically adjacent horizontal extrema) greater than 0.667 in either the (x, z) or (y, z) coordinate plane are excluded. However, frequently there are neighbour vorticity patches of the same sign whose connecting slope is greater than this. Since there are important dynamical processes of both amalgamation by attachment and fragmentation by vertical straining, these patches can either join or further separate at a later time. If a less stringent upper bound were placed on the local slope, the analysis would yield fewer independent vortices with larger heights, although the sensitivity to this bound becomes quite small at late times. In the absence of an excessive slope, Δ defines the boundary of the vortex in the vertical, as it also does in the horizontal (see below); we choose $\Delta = 0.2$ as in V2D.

C. *Eliminate redundancy among axes* There are no redundant points among any of the axes of selected vortices.

Procedure During the axis search (B above), if another three-dimensional

extremum of lesser amplitude (greater n) is encountered, it is grafted onto the axis of the stronger extremum and deleted as an independent extremum. After calculating all axes using this procedure, an additional test is made for whether there are any points which are in common between two or more axes; if so, from among the associated three-dimensional extrema, only the strongest is retained as the core of an independent axis, which is then recomputed from among the associated axes by searching outward from the new core and always choosing the longest branch (or, if equal length, the branch with the strongest extremum) at each intersection point.

Comments The dynamical processes of axisymmetrization and alignment act against the persistence of multiple branches, although they permit multiple cores (three-dimensional extrema) on the axis. The choice of whether to select the longer or stronger branch is an arbitrary one, but it only rarely needs to be made and thus is of little consequence in determining population-averaged vortex properties.

Once non-redundant axes have been determined, we measure the bulk properties of height and slope (tilt from the vertical) from each vortex. Above the central extremum, we define h_u as the vertical distance from the top grid point of the axis to the central extremum plus 0.5dz (which is either halfway to the next grid point or the distance to the vertical boundary), and we define s_u as the ratio of horizontal and vertical displacements between these two points, unless they are the same point, in which case $s_u = 0$. Analogous quantities, h_l and s_l, are defined below the central extremum. The vortex height h represents a centre-to-edge distance, where possible not limited by intersection with a vertical boundary. Thus, it is equal to the average of h_u and h_l, unless one of the axis ends intersects a boundary, in which case h is the non-intersecting half-height, or both ends intersect the boundaries, in which case h is the larger half-height. The vortex slope s is defined as the maximum of s_u and s_l.

D. *Identify interior and boundary regions* In the horizontal plane of the central extremum, a vortex has a simply connected region with vorticity of the same sign as its extremum.

Procedure The vortex interior is the simply connected set of grid points V_n satisfying (1) in the plane of the central extremum, and δV_n is the set of grid points defining its outer boundary. The procedure for finding these sets is presented in V2D.

E. *Eliminate horizontal redundancy* All independent vortices are spatially separate in their associated horizontal interior regions (i.e. planes).

Procedure If any three-dimensional extremum lies within the interior set V_n of another vortex with a stronger extremum, the former is discarded as an independent vortex.

Comments The two redundancy tests, C and E, admit the possibility that two vortices with central extrema at different levels have an intersection between the axis of one and the plane of the other, and perhaps vice versa as well. This is interpreted as separate but closely interacting vortices, and it is never a persistant state under the action either of axisymmetrization and alignment or of fragmentation.

F. *Test horizontal shape* The vorticity distribution in the horizontal plane of the central extremum should not depart excessively from axisymmetry.

Procedure For each candidate vortex the following shape properties are calculated:

$$C = \sum_{\delta V} \mathrm{d}s, \tag{2}$$

$$A = \sum_{V} \mathrm{d}s^2, \tag{3}$$

$$\delta x_i = \frac{\sum_V \mathrm{d}s^2 w(x_i - x_{ni})}{\sum_V \mathrm{d}s^2 w}, \tag{4}$$

$$M_{ij} = \frac{\sum_V \mathrm{d}s^2 w(x_i - x_{ni})\,(x_j - x_{nj})}{\sum_V \mathrm{d}s^2 w} \tag{5}$$

These quantities are, respectively, the circumference, the area, the first spatial moment or centroid displacement, and the second-moment matrix. i and j are horizontal coordinate indices (i.e. $(x_1, x_2) = (x, y)$), and w is a weighting factor equal to either 1 or ζ. M_{ij} has positive eigenvalues $\lambda_1 \geqslant \lambda_2$.

Using these quantities, the following tests are made:

$$C \leqslant C_{\max}, \tag{6}$$

$$A \leqslant A_{\max}, \tag{7}$$

$$r \equiv (A/\pi)^{\frac{1}{2}} \geqslant r_{\min}, \tag{8}$$

$$R \equiv \frac{C}{2\pi^{\frac{1}{2}} A^{\frac{1}{2}}} \leqslant R_{\max}, \tag{9}$$

$$\delta \equiv \frac{(\delta x_1^2 + \delta x_2^2)^{\frac{1}{2}}}{r} \leqslant \delta_{\max}, \tag{10}$$

$$\epsilon \equiv \left(\frac{\lambda_1}{\lambda_2} - 1\right)^{\frac{1}{2}} \leqslant \epsilon_{\max}. \tag{11}$$

Candidate vortices failing any of these tests are rejected.

Comments The tests (6)–(11) are identical to the horizontal shape tests in V2D. We also choose quite similar values for the threshold parameters: $C_{\max} = 0.5 \times 8\pi$, $A_{\max} = [0.2 \times 2\pi]^2$, and $r_{\min} = \mathrm{d}s = 0.0327$ are all larger than their counterparts in V2D, approximately in proportion to the ratio of resolution lengths, $\mathrm{d}s$, and $R_{\max} = 1.75$, $\delta_{\max} = 0.35$, and $\epsilon_{\max} = 2.5$ are identical. The selection tests are made with both values of w, but, unless otherwise stated, the analysed properties quoted below are those with $w = 1$.

After all this, a set of N_{v} coherent vortices has been selected, and many of their important properties have been determined.

3. Vortex properties

The selection procedure yields N_{v} coherent vortices from among N_{e} three-dimensional vorticity extrema. The selection ratio $N_{\mathrm{v}}/N_{\mathrm{e}}$ is plotted in figure 2 as a function both of time and vortex amplitude ζ_{v} ($= |\zeta_n|$). At $t = 0$, this ratio is quite small, although larger than the initial ratio in V2D because of the coarser resolution here, hence the lower wavenumber bandwidth of the initial state, and hence its lower structural complexity and distortion from the vortex archetype. In any event, the selection ratio subsequently declines to a value of less than 0.1 (similar to the minimum in V2D) within the first few eddy circulation times t_{c} ($= 1/\mathrm{rms}\zeta = 0.025$ at $t = 0$; see DGT). This initial decline is due to the mutual straining among the nearly contiguous, incipient vortices which deform vorticity patterns away from the

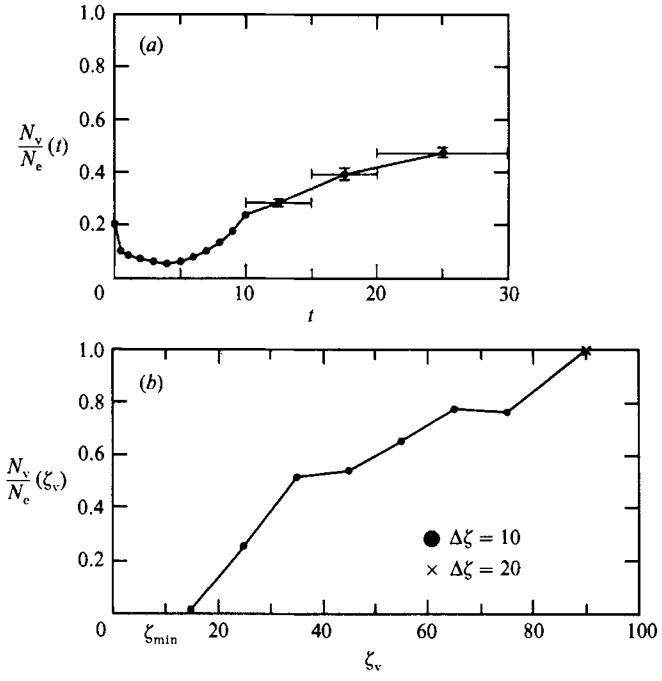

FIGURE 2. Selection ratio for vortices, N_v/N_e: (*a*) time evolution and (*b*) dependence on vortex amplitude ζ_v ($=|\zeta_n|$). In (*a*) values are plotted for individual times for $t \leqslant 10$ and for time averages thereafter; the averaging intervals are indicated by the horizontal lines and the vertical lines are error bars equal to the standard deviation divided by the square root of the number of individual values at unit times in the average. For (*b*) the values are averages over all vortices in the indicated ζ_v intervals and over all unit times from $t = 8$ to $t = 12$.

statistically isotropic initial conditions. Thereafter, the selection ratio steadily increases as the vortices emerge and then become spatially sparse, which diminishes the straining rates among vortices. At late times, $N_v/N_e \approx 0.5$, which is substantially less than the comparable value in V2D. However, in a three-dimensional solution, many extrema are not accepted as independent vortices because they are vertically connected to stronger extrema; if we multiply the selection ratio by the average number of three-dimensional extrema on an axis n_c (figure 10*a*), we obtain a late-time selection ratio similar to V2D. Finally, as in V2D, the selection ratio increases with amplitude (figure 2*b*): in a given ambient strain field, stronger vorticity extrema are more likely to axisymmetrize and align themselves and thus be accepted as coherent vortices.

The vortex abundance is shown in figure 3. $N_v(t)$ steadily decreases by the vortex removal proccsses of strain-enhanced dissipation, merger, and attachment. After an initial period of vortex emergence, lasting a few eddy circulation times, the abundance has approximately the form of a power-law decay, $N_v \propto t^{-\alpha}$, with α perhaps somewhat larger than 1 (see the comparison curves in figure 3). This is also true in V2D, except the value of α is significantly smaller there. In either two- or three-dimensional domains, the value $\alpha = 1$ corresponds to an entirely random rate of close encounters between sparse vortices, with vortex removal presumed to occur for some fraction of these close encounters (see V2D, equation (19)). Thus, figure 3 suggests that close approaches among geostrophic vortices may be more frequent than for entirely random, mutually uncorrelated trajectories, in contrast to the two-

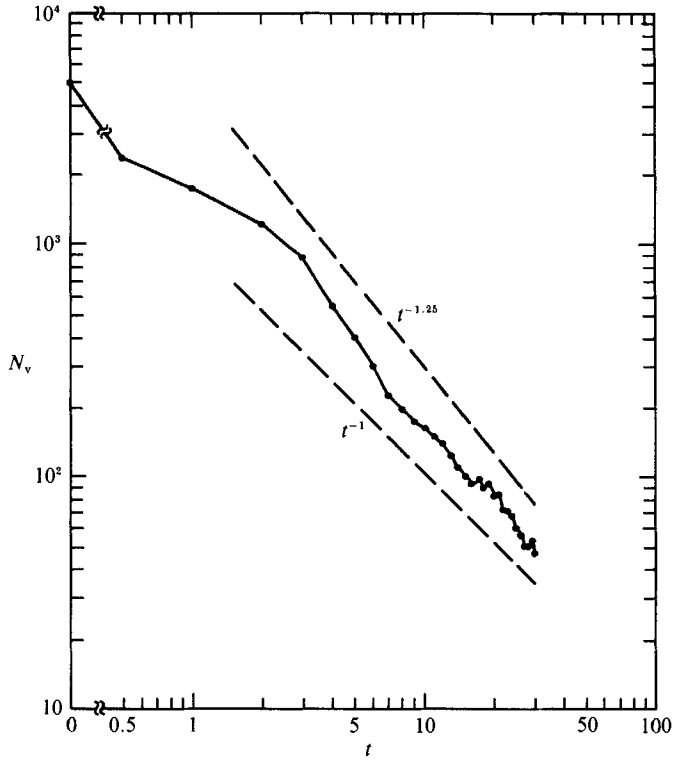

FIGURE 3. Evolution of the vortex population $N_v(t)$. Dashed lines are power-law decay curves for comparison.

dimensional case where the encounter rate is clearly less frequent than random. The vortex trajectories are dynamically controlled through mutual advection, and as yet no theoretical estimates have been made for the rates of encounter due to this process, neither for two-dimensional nor for geostrophic motions. It is also true here that vortex heights are typically larger than their radii even after normalization by N/f, where N is the buoyancy frequency and f is the rotational frequency (see figures 7–9). So vertical separation distances between vortices are smaller than horizontal ones; thus, by this measure, vortices are less sparse in z than in (x, y), which may contribute to an enhancement of their frequency of close approaches in geostrophic turbulence relative to two-dimensional turbulence. Also, in addition to merger, there is the process of attachment in geostrophic turbulence that can enhance the rate of disappearance of independent vortices.

The distribution of the vortex population with amplitude is shown in figure 4. It is qualitatively quite similar to its counterpart in V2D. The distribution has a broad bandwidth at all times, although the bandwidth decreases with t both because viscous amplitude decay reduces the maximum ζ_v and because the relatively more rapid removal of weaker vortices through non-conservative close encounters diminishes the population at small ζ_v. The primary vortex generation mechanism in this solution is emergence through axisymmetrization and alignment around the vorticity extrema present in the initial conditions, and this accounts for the broad maximum in $N_v(\zeta_v)$ at intermediate ζ_v. At moderately early times (e.g. $t = 3$ in figure 4), there is also a peak in the distribution for small ζ_v that is not present in the initial

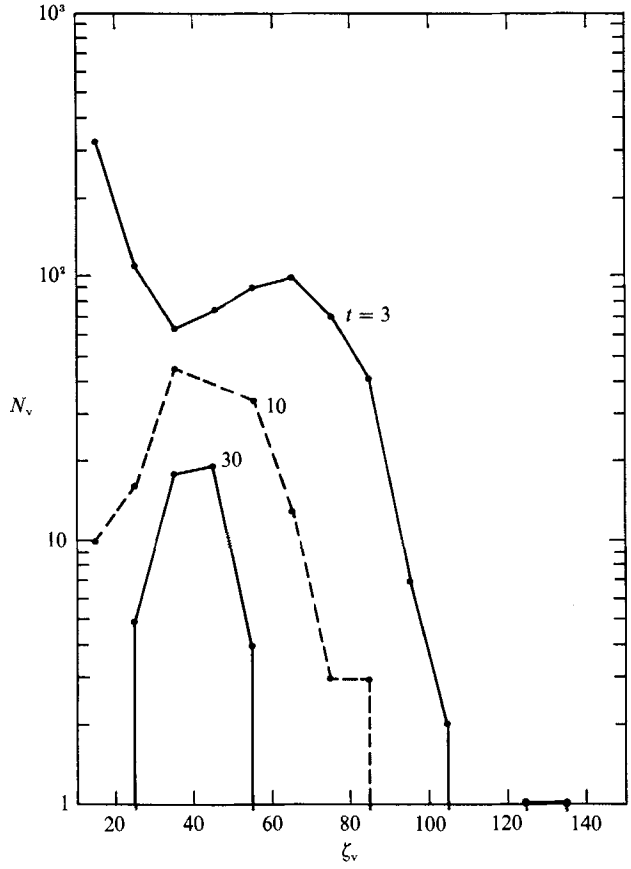

FIGURE 4. Amplitude distribution of the selected vortices $N_v(\zeta_v)$ grouped in intervals of $\Delta\zeta_v = 10$. Vertical line segments indicate that no vortices exist outside the indicated interval.

conditions. As in V2D, these weaker vortices arise from a secondary generation process of vortex emergence from the vorticity filaments and fragments created by close interactions between stronger vortices.

An intrinsically three-dimensional effect is illustrated in figure 5. On approximately the same timescale as vortex emergence, an inhomogeneity develops in the vertical distribution of vortex central extrema: they are relatively more likely to occur at the vertical boundary levels and less likely to occur in the adjacent intervals near the boundaries. This bears a direct relation to the boundary maxima in vorticity variance (DGT, figures 11 and 12). A partial explanation for this distribution is that there is an evolutionary tendency for a geostrophic vortex whose central extremum is initially near a boundary to shift it towards the boundary under the action of a time-varying vertical strain field of moderate amplitude. This process probably has its cause in the vertical boundary condition for this solution, $\partial\psi/\partial z = 0$, which is generally conducive to boundary extrema in ψ or ζ. (ψ is the geostrophic stream function, related to vorticity by $\zeta = \psi_{xx} + \psi_{yy}$.) It is interesting that the average vortex amplitude $\langle\zeta_v\rangle$ (z) (not shown) is not significantly inhomogeneous in z, in spite of the non-uniform abundance. ($\langle\cdot\rangle$ denotes an average over the vortex population, either *in toto* or in some partition, as here in the central location z_n.)

The evolution of vortex amplitudes ζ_v is shown in figure 6. The only qualitative

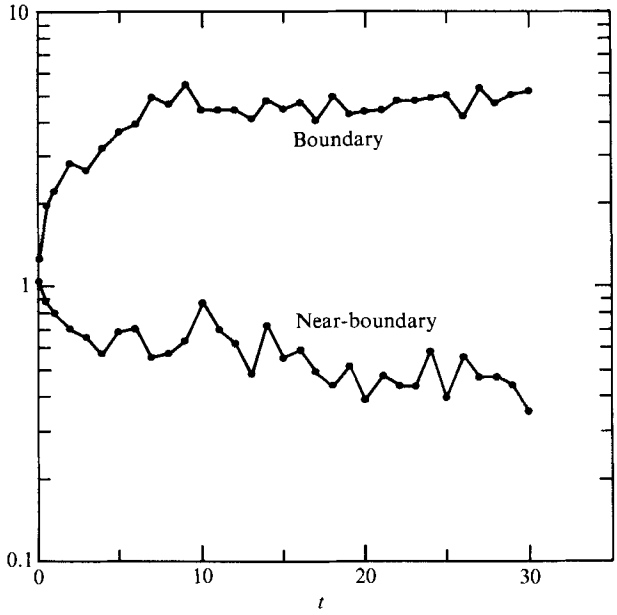

FIGURE 5. Relative frequency of occurrence of vortex central extrema either on the grid levels closest to the vertical boundaries (i.e. $p = 0$ and $N_z - 1$ in the notation of DGT, equation (11)) or on the two adjacent interior levels near the boundaries (i.e. $p = 1$, 2, $N_z - 3$, and $N_z - 2$). The quantities plotted are equal to $N_v^* \pi / N_v \Delta z^*$, where the asterisk denotes the vortex abundance and associated vertical interval for these levels (i.e. $2\pi/N_z$ and $4\pi/N_z$, respectively).

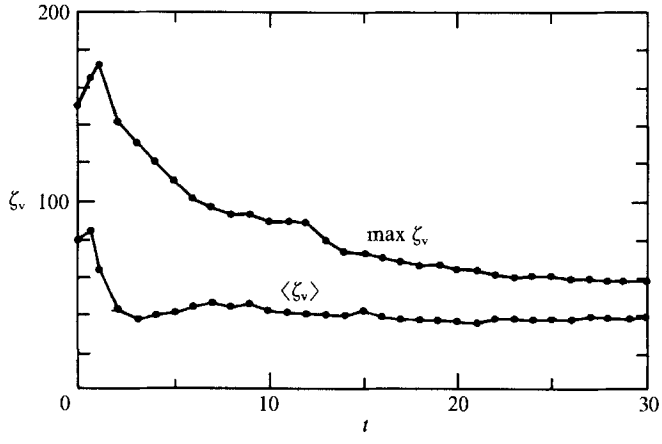

FIGURE 6. The maximum and average vortex amplitudes, $\max \zeta_v$ and $\langle \zeta_v \rangle$.

difference with its counterpart in V2D is the amplitude growth during the first few eddy circulation times. This results from the conversion of stretching vorticity η $(= (f^2/N^2)\psi_{zz})$ to relative vorticity ζ at the extrema of their sum, the potential vorticity q. The latter is a conserved quantity for inviscid quasi-geostrophic dynamics (DGT, equation (1)). Of course, this conversion of potential vorticity components is precluded in two-dimensional flow where $\zeta = q$. Alternatively expressed, in geostrophic turbulence there is a rapid initial growth in vortex height (figure 8*a*), which diminishes η. This is also reflected in the early-time evolution of the centroid wavenumber for the enstrophy spectrum (DGT, figure 3). The

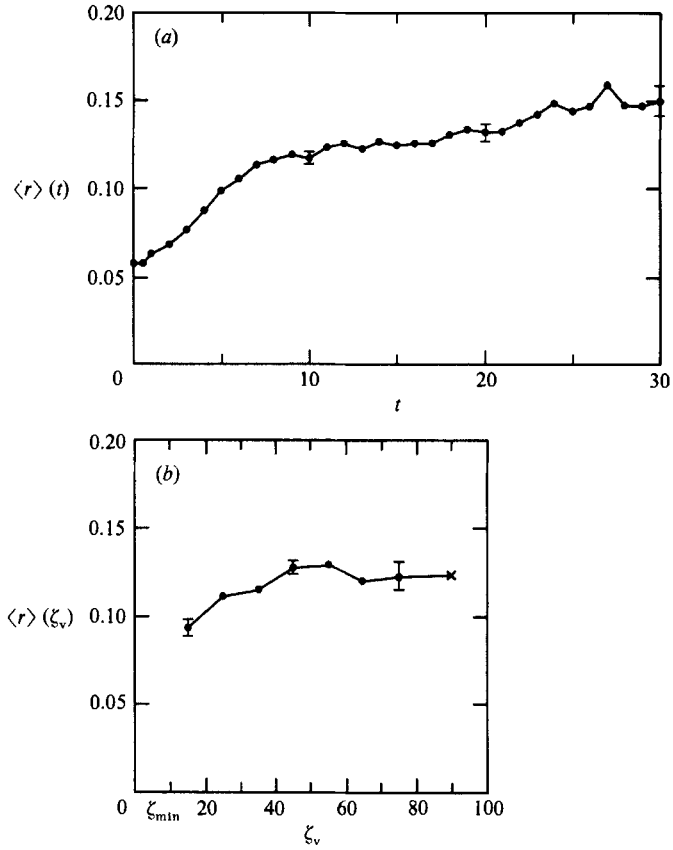

FIGURE 7. Average vortex radius $\langle r \rangle$: (*a*) time evolution and (*b*) dependence on amplitude. In (*a*) the average is over all vortices at a particular time. In (*b*) the average is over all vortices within the indicated amplitude interval and the time interval $8 \leqslant t \leqslant 12$, and dots and crosses indicate an amplitude interval of $\Delta\zeta_v = 10$ and 20, respectively. Error bars are the standard deviation divided by the square root of the number of vortices in the average.

subsequent decay of $\max/\zeta_v(t)$ in figure 6 reflects the dominance of viscous effects over vortex stretching, at least for the strongest vortices. Viscous diffusion is always acting on the vortices, albeit weakly, while vortex stretching is restricted to intermittent events of strong vertical straining during close encounters between vortices, which become increasingly rare as the vortices become sparser. The average amplitude $\langle \zeta_v \rangle$ (t) is nearly constant after an initial cycle of growth by stretching and viscous decay. This reflects an approximate balance between the viscous decay of individual vortices and the selective removal of weaker vortices which tends to raise the average amplitude, as is also true in V2D.

Vortex size grows with time, in both the horizontal (figure 7*a*) and the vertical (figure 8*a*), owing to the amalgamation processes of merger and attachment and to the selective destruction by straining of the weaker vortices that are smaller (figures 7*b* and 8*b*). Horizontal size can also grow by viscous diffusion, but vertical size cannot grow in this way since there is no vertical viscosity in this particular solution. However, as in V2D, we conclude that diffusive spreading by itself is a secondary effect, since the life histories of individual vortices show r and h changing nearly discontinuously in time during events of close interaction among vortices. (A life history was presented in V2D, §5.) Of course, viscosity does play an essential role in

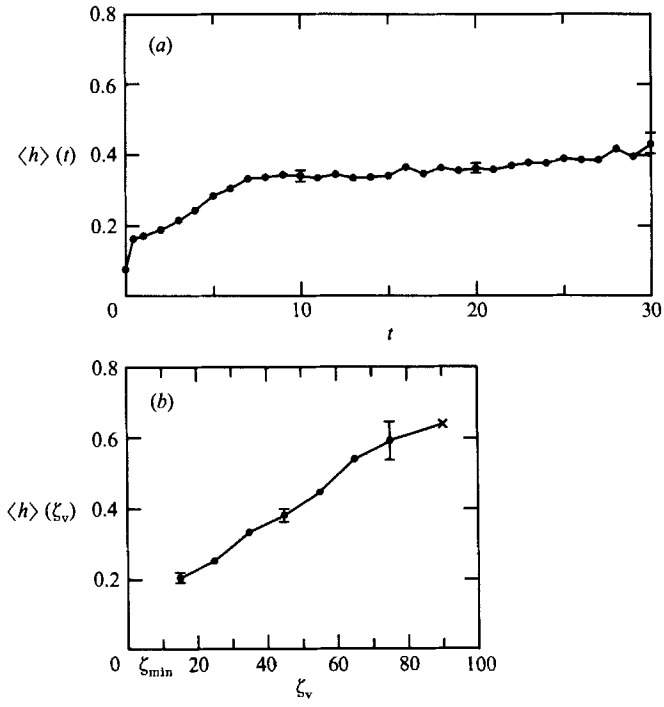

FIGURE 8. Average vortex half-height $\langle h \rangle$. Plotting conventions are as in figure 7.

the processes of axisymmetrization and alignment, as they act to complete the merger and attachment events, but this is a strain-enhanced diffusion and dissipation whose characteristic time is $t_Z = t_c \ln Re$, where Re is the Reynolds number, which is much shorter than the diffusive time $t_\nu = t_c Re$ (Lesieur 1987, p. 194). For the present solution, we can estimate t_ν by $1/\nu\langle k \rangle_T^4(t=0) = 25$, where $\langle k \rangle_T$ is the centroid horizontal wavenumber for the energy spectrum; see DGT. Thus, with the definition $Re = t_\nu/t_c$, Re has the value 10^3 here, and $t_Z = 0.17$.

It is quite rare for the merger and attachment events to cause a decrease in r, but h can have nearly discontinuous changes of either sign. The associated vertical processes are attachment and fragmentation; under the action of vertical straining, the latter process often severs a vortex axis at the same level where the former had previously joined two vortices. Evidently, however, attachment events are more common than fragmentation events, since $\langle h \rangle (t)$ increases. $\langle r \rangle$ and $\langle h \rangle$ grow more rapidly at moderately early times when the vortex density is greater and close encounters are more frequent. In addition, there is a large increase (more than a doubling) in $\langle h \rangle$ in the first few eddy circulation times due to vorticity alignment and attachment, although I do not know the reason for its rapidity. Finally, figures 7(*b*) and 8(*b*) show a positive correlation between vortex amplitude and size.

As discussed in DGT, many properties of geostrophic turbulence are approximately isotropic in the spatial coordinates $(x, y, (N/f)z)$. Thus, we examine the vortex aspect ratio h/r with a normalization by N/f (figure 9). Except for the first few eddy circulation times, when $\langle h/r \rangle$ rapidly increases because $\langle h \rangle$ does, there is very little change in the aspect ratio with time, even with the considerable growth in size (figures 7 and 8) and strong dependence on vortex amplitude (figure 9*b*). This is yet another aspect of approximate three-dimensional isotropy of geostrophic turbulence.

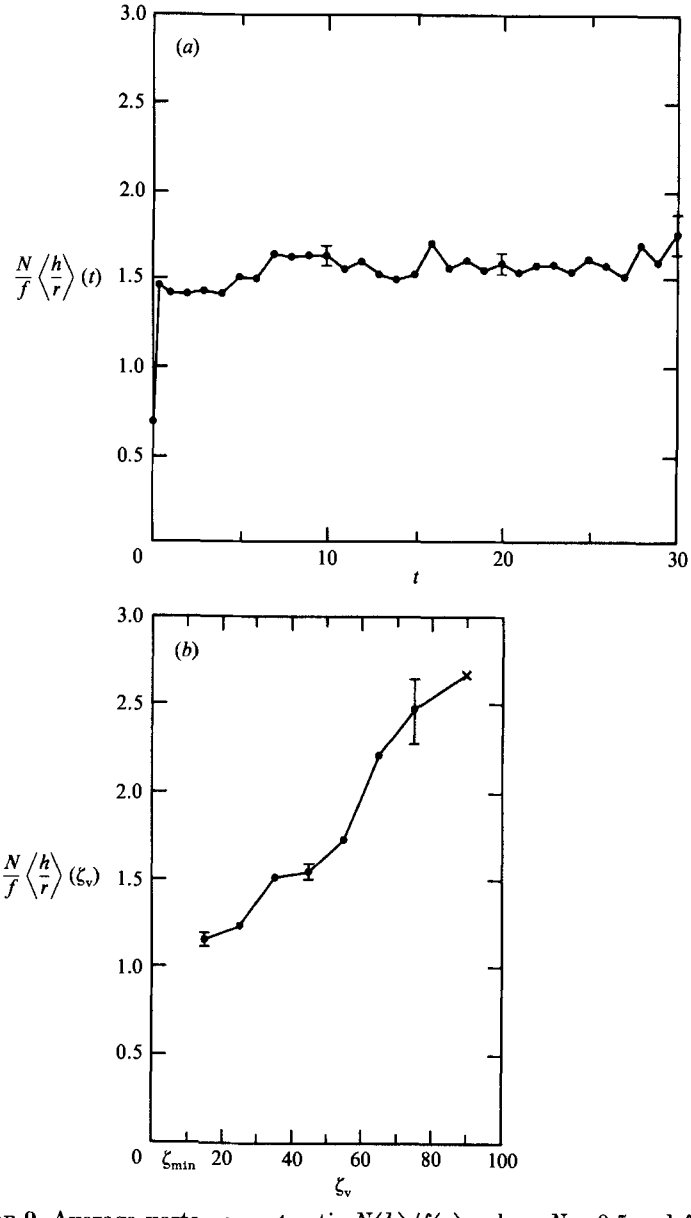

FIGURE 9. Average vortex aspect ratio $N\langle h\rangle/f\langle r\rangle$, where $N = 0.5$ and $f = 1$ for solution A. Plotting conventions are as in figure 7.

As with the other properties analysed in DGT, §11, the particular values of the normalized aspect ratio do not vary much with N or f. These values, $1 \lesssim Nh/fr \lesssim 3$, are intermediate between the much smaller values at which baroclinic instability typically occurs and the somewhat larger values at which internal barotropic instability usually occurs (McWilliams 1990*b*); the latter process is additionally inhibited for the vortices by the weakness of the large-radius reversal in their horizontal vorticity gradient (figure 13), which is the instability source (Gent & McWilliams 1986).

The attachment process between initially separate vortices usually preserves their

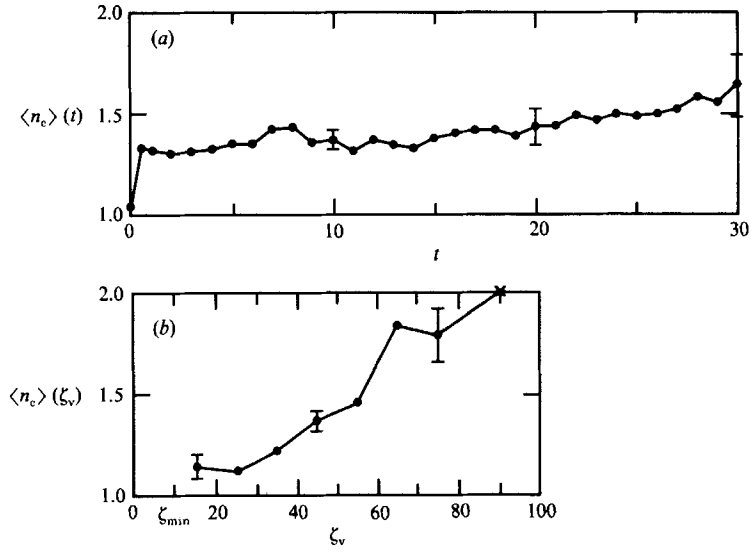

FIGURE 10. Average number of three-dimensional extrema on a vortex axis $\langle n_c \rangle$. Plotting conventions are as in figure 7.

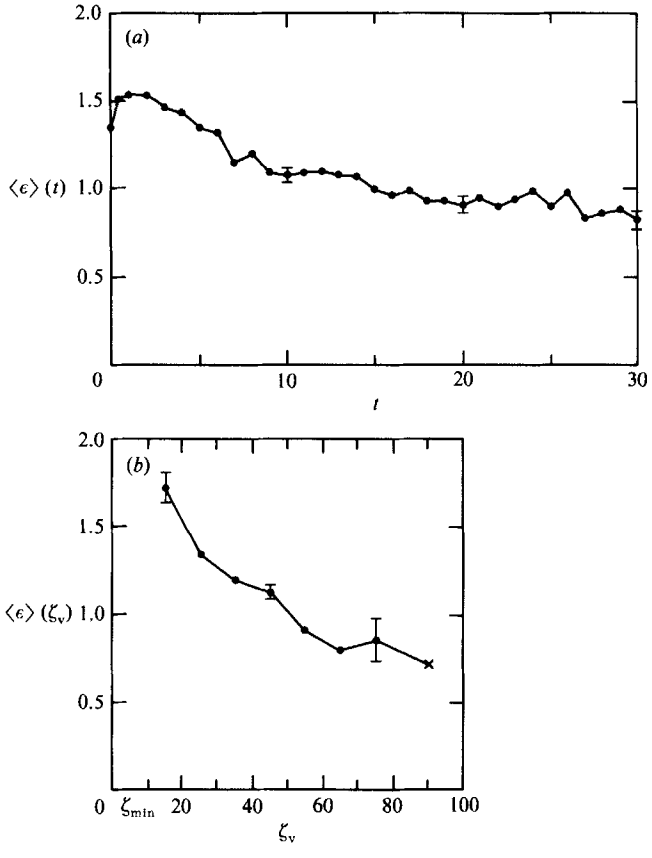

FIGURE 11. Average vortex ellipticity $\langle \epsilon \rangle$. Plotting conventions are as in figure 7.

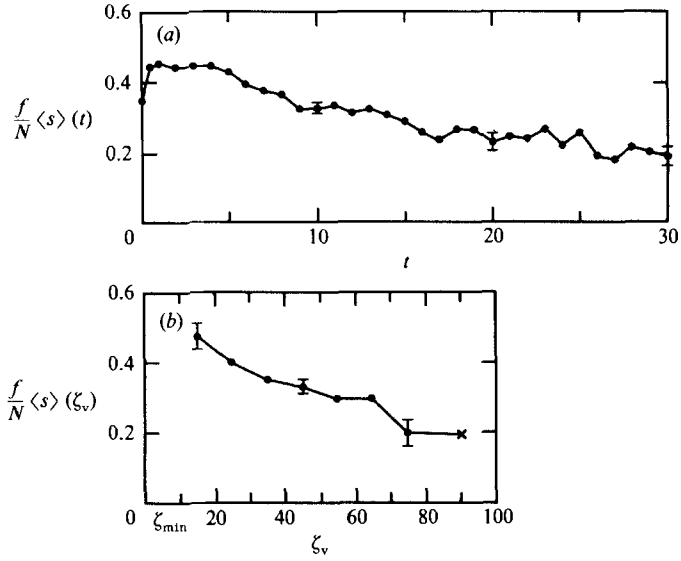

FIGURE 12. Average vortex slope $(f/N)\ \langle s\rangle$. Plotting conventions are as in figure 7.

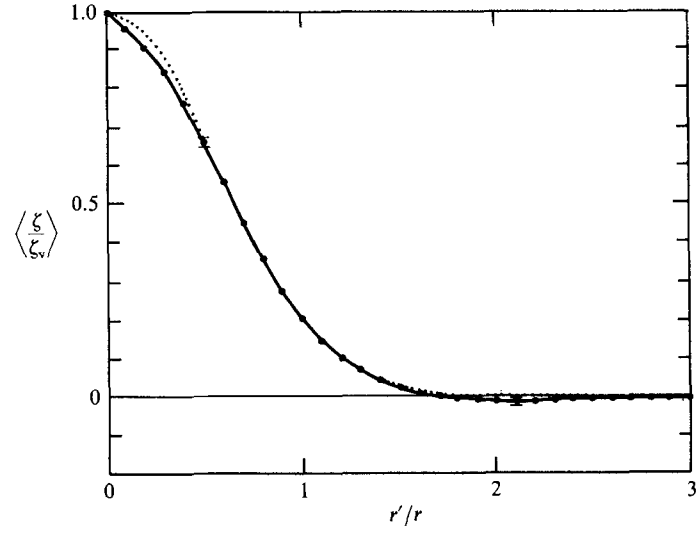

FIGURE 13. Average radial profile for the best-shaped vortices (see text). The dotted line is a Gaussian profile, $\exp[-a(r'/r)^2]$, with $a = 1.609$ such that it has the value $A = 0.2$ at $r' = r$. Error bars are the standard deviation at each radius divided by the square root of the number of vortices in the average over the population of stringently selected vortices during $20 \leqslant t \leqslant 30$.

central extrema as independent three-dimensional extrema. We define n_c as the number of independent extrema on a vortex axis. Figure 10(*a*) shows the increase of $\langle n_c\rangle$ with time due to the occurrence of attachment events, including the same rapid increase in the first few eddy circulation times seen above in $\langle h\rangle$ and $\langle h/r\rangle \cdot \langle n_c\rangle$ also is a strong function of amplitude (figure 10*b*), indicating that the stronger vortices undergo more attachment events (and fewer vertical fragmentation events) and thus attain greater heights and aspect ratios.

Mutual straining among vortices, particularly those in close proximity, causes

shape deformations away from the posited ideal. These deformations are resisted, or subsequently recovered from, through the organizing processes of axisymmetrization and alignment. In figures 11 and 12 are two measures of deformation: the horizontal ellipticity ϵ in the plane of the central extremum, and the axis slope fs/N normalized in a manner appropriate to the dynamically isotropic coordinates. For both measures (as for ϵ in V2D), the behaviour is quite simple: deformations initially increase during the first few eddy circulation times as closely packed vorticity centres strain each other strongly; after vortex emergence, however, increasing vortex sparseness leads to decreasing strain and deformation. Deformations decrease with vortex amplitude, as one expects from simple solutions of vortices in a strain field (e.g. Moore & Saffman 1971). One noticeable difference with V2D is that the value of $\langle\epsilon\rangle$ is uniformly larger in the geostrophic turbulence solution. This might be attributed to the additional source of strain, S_{v}, which induces elliptical deformations of the vortex in horizontal planes as well as tilting of its axis.

In V2D (§6), power-law fits ($\propto t^{\alpha}$) were made to the vortex properties, and the resulting exponents were used to test simple model predictions of vortex population evolution. Although it seems to me premature to declare models for geostrophic population evolution, it may be useful to describe the vortex properties in terms of their exponents. Fits during the time interval $5 \leqslant t \leqslant 30$ yield the following:

$$\left.\begin{aligned} \alpha_N = -1.16, \quad \alpha_r = 0.22, \quad \alpha_\Gamma = 0.37, \\ \alpha_\xi = -0.13, \quad \alpha_\epsilon = -0.24, \quad \alpha_s = -0.47, \\ \alpha_{h/r} = 0.008, \quad \alpha_{n_c^{-1}} = 0.26. \end{aligned}\right\} \tag{12}$$

Γ is the circulation of a vortex (see (18) of V2D for its definition).

As discussed above, the exponent for N_{v} is appreciably more negative in this geostrophic turbulence solution than in V2D. On the other hand, the exponents for $\langle r\rangle$, $\langle\Gamma\rangle$, $\langle\zeta_{\mathrm{v}}\rangle$, and $\langle\epsilon\rangle$ are rather similar to their counterparts in V2D. Furthermore, the exponent for $\langle\epsilon\rangle$ also decreases with time when fits over shorter time intervals are made, as expected from simple models of deformation due to horizontal strain, S_{h} (see V2D).

Finally, we examine another aspect of vortex shape, the radial profile $\zeta(r')$, where r' is the radial coordinate measured from the vortex centre. There is much variability in individual profiles, because the intermittent non-conservative events change the profile in ways that are sensitive to details of the particular interactions. Nevertheless, there is a favoured radial profile for vortices whose shape is close to the archetype, presumably because they have had a long interval, of order t_Z, to recover from the last close encounter. We educe this profile in the same way as in V2D. First we select those vortices which have the least distortion from axisymmetry. We do this with a more stringent set of selection parameters: $r_{\min} = 0.06$, $R_{\max} = 1.25$, $\delta_{\max} = 0.1$, and $\epsilon_{\max} = 0.5$. The more stringent selection procedure yields $N_{\mathrm{s}}(t)$ ($\leqslant N_{\mathrm{v}}(t)$) vortices. This number varies little with time after emergence, with a value around 10, as the decline in N_{v} (figure 3) approximately balances the decline in distortion (figures 11 and 12). For each of the stringently selected vortices, an azimuthal average is performed within radial intervals of $\Delta r' = 0.75\mathrm{d}s = 0.0245$, and then the result is normalized by its extremum ζ_n and interpolated onto a normalized radial coordinate $r'' = r'/r$, on a uniform grid with a resolution length of $\Delta r'' = 0.1$. Next we take an average over both the population of stringently selected vortices and over a time interval well after emergence (i.e. for all unit times $20 \leqslant t \leqslant 30$). The result is shown in figure 13. The average vortex profile is close to a Gaussian shape,

except very near the centre and at large radii, where the average profile lies below the Gaussian one. In these properties it is quite similar to V2D. The discrepancy near the centre is somewhat larger here than in V2D, perhaps owing to the poorer horizontal resolution (NB $\langle r \rangle / \mathrm{d}s$ is smaller here by about one-third). The discrepancy with the Gaussian profile on the edge of the vortex is associated with a zone with vorticity of opposite sign, which is not true in V2D, but its amplitude is far less than would fully shield the vortex core by making the total circulation (i.e. $\int_0^\infty \zeta(r')\, r' \mathrm{d}r'$) zero; for example, the shielded Gaussian profile, $\zeta(\rho) = (1-\rho^2)\mathrm{e}^{-\rho^2}$, has a minimum value of -0.14, nearly ten times larger than in figure 13. The development of an approximately Gaussian profile is interpreted as a consequence of viscous diffusion (see V2D).

We might also examine the vertical profile of vortices. However, there is so much variety due to multiple cores and vertical boundary effects that no universal shape is found. On the axis vorticity decays away from the three-dimensional extrema, and I find no good evidence for connected zones of opposite-sign vorticity beyond the ends of the axis.

4. Discussion

In this paper a methodology is presented for the identification of the coherent vortices in a numerical solution for decaying geostrophic turbulence. In addition, various vortex properties are measured and analyses are made for the property distributions within the vortex population and for their time evolution.

The principal results are the following. The vortices emerge from random initial conditions; initially, the fraction of vorticity extrema selected as coherent vortices is small, but it increases steadily with time. The selection ratio is also a monotonic function of vortex amplitude. The vortex population decreases with time owing to non-conservative vortex interactions during close encounters; the rate of decrease is close to, but somewhat faster than, that of a purely random rate of encounter. Vortices with weaker amplitudes are more likely to be destroyed by strain or absorbed by merger or attachment. Vortex amplitudes decrease owing to diffusion, whose rate is often enhanced by deformation in response to strain. Vortex centres have an inhomogeneous distribution in the vertical: vertical boundaries are a particularly common location for centres, and the neighbouring levels are a particularly uncommon one. Vortex size increases with time, both vertically and horizontally; this occurs primarily through merger and attachment interactions, although horizontal diffusion also contributes to horizontal spreading. Nevertheless, the normalized aspect ratio $N/f \langle h/r \rangle$ changes very little with time after the initial period of vortex emergence. The stronger vortices tend both to be larger in size and to have a larger aspect ratio. The latter suggests that stronger vortices are relatively more successful in attachment events, as does the greater number of three-dimensional extrema on their axis n_c. Deformations of vortices from their preferred shape, which is axisymmetric and aligned, decrease with both time and vortex amplitude. This is consistent with a vortex's deformation varying directly with the strain field from other vortices, which are increasingly distant with time on average, and varying inversely with its own vorticity amplitude. Finally, the average radial profile for vortices which are not strongly deformed is close to a Gaussian shape, and this is attributed to the slow but persistent influence of diffusion.

It is remarkable that this behaviour is similar in so many ways to the vortices of two-dimensional turbulence (as presented in V2D). In making this comparison, of

course, one must exclude the attributes referring to the added vertical dimension of geostrophic turbulence (i.e. $N_v(z), \langle h \rangle, N/f\langle h/r \rangle, n_c$, and $f/N\langle s \rangle$). However, the distributions of the horizontal properties of the vortices and their evolution do indeed seem quite similar (i.e. $\max \zeta_v, \langle \zeta_v \rangle$, $\langle r \rangle$, $\langle \epsilon \rangle$, and $\langle \zeta/\zeta_v \rangle$ (r'/r). (We cannot yet go beyond a declaration of qualitative similarity at present, because the solutions analysed here and in V2D are not quantitatively equivalent in numerical parameters and initial conditions.) Some differences do occur in the vortex population measures. The selection ratio N_v/N_e is smaller in geostrophic turbulence because of multiple extrema on the vortex axes, though this difference largely disappears for the quantity $\langle n_c \rangle$, N_v/N_e. The vortex abundance $N_v(t)$ does decay somewhat more rapidly in geostrophic turbulence, suggesting a possibly qualitative difference in the rate of vortex close encounters compared to two-dimensional turbulence, and, as a consequence, the average horizontal deformation $\langle \epsilon \rangle$ (t) also decays more rapidly. Nevertheless, the shape of the amplitude distribution $N_v(\zeta_v)$ is similar between the two types of flow.

In summary, the coherent vortices of geostrophic turbulence exhibit an orderly evolution in their property distributions, and this encourages the hope that a useful turbulence theory can be developed based upon vortex dynamics.

The National Center for Atmospheric Research is sponsored by the National Science Foundation.

REFERENCES

CHARNEY, J. 1971 Geostrophic turbulence. *J. Atmos. Sci.* **28**, 1087–1095.

FLIERL, G. 1988 On the instability of geostrophic vortices. *J. Fluid Mech.* **197**, 349–388.

GENT, P. & MCWILLIAMS, J. 1986 The instability of barotropic circular vortices. *Geophys. Astrophys. Fluid Dyn.* **35**, 209–233.

LESIEUR, M. 1987 *Turbulence in Fluids.* Martinus Nighoff, 286 pp.

MCWILLIAMS, J. 1989 Statistical properties of decaying geostrophic turbulence. *J. Fluid Mech.* **198**, 199–230 (referred to as DGT herein).

MCWILLIAMS, J. 1990*a* The vortices of two-dimensional turbulence. *J. Fluid Mech.* **219**, 361–385 (referred to as V2D herein).

MCWILLIAMS, J. 1990*b* Geostrophic vortices. In *Proc. Intl School of Physics Enrico Fermi.* Italian Physical Society (in press).

MOORE, D. & SAFFMAN, P. 1971 Structure of a line vortex in an imposed strain. *Aircraft Turbulence and its Detection*, pp. 339–354. Plenum.

POLVANI, L. 1990 Two-layer geostrophic vortex dynamics. Part 2. Alignment and two-layer V-states. *J. Fluid Mech.* (in press).

RHINES, P. 1979 Geostrophic turbulence. *Ann. Rev. Fluid Mech.* **11**, 401–411.